Radioactive Exploration Using Image Processing Techniques of Spectrometric Data, Central Eastern Desert, Egypt

Adel Zein Bishta

Faculty of Earth Sciences, King Abdulaziz University, Jeddah, Saudi Arabia
abishta@kau.edu.sa

Abstract: The central part of the Eastern Desert of Egypt is mainly covered by complex of late Proterozoic igneous and metamorphic rocks. Some important occurrences of radioactive mineralization were discovered in this area by the Egyptian Nuclear Materials Authority. Different techniques of gamma-ray spectrometry and image processing, as well as field investigations are applied in this work, aiming to define new occurrences of the possible radioactive mineralization. The constructed false color composite Landsat ETM+ image showed the main lithologic units of the investigated area. The structural lineaments of the study area are extracted from the digital ETM+ data. Statistical analysis of these lineaments revealed that the predominant trends are NW, NE, N-S, NNW and NNE with a minor trend in E-W direction. The image processing technique is used in constructing gamma-ray spectrometry color raster maps of K, eU, eTh and TC. These color raster maps distinguished to some extent the different mapped rock units according to their K-contents. These maps helped in identifying the zones of high radioactivities, which are confined to late-tectonic younger granitic intrusions and the Phanerozoic phosphatic deposits. The processed colored enhanced linear stretched ternary map illustrates five -color groups which interpreted as being five different radioactive units (R1 to R5). These radioactive units reflect the different concentrations of the three radioelements (K, eU and eTh) characterizing each radioactive occurrence. R5-type indicates to uranium enrichment while R2-type reflects thorium enrichments. The ternary map pointed to the important new areas of uranium occurrences located in the study area, such as El Missikat and El Erediya plutons and the phosphatic beds of Wadi Safaga. It is showed also that, the plutons of Kab Amiri, El Missikat and Wadi El Markh younger granitic intrusions are exhibiting thorium enrichments.

[Adel Zein Bishta. **Radioactive Exploration Using Image Processing Techniques of Spectrometric Data, Central Eastern Desert, Egypt.** *Life Sci J* 2017;14(11):102-113]. ISSN: 1097-8135 (Print) / ISSN: 2372-613X (Online). http://www.lifesciencesite.com. 15. doi:10.7537/marslsj141117.15.

Keywords: Image processing; lineaments extraction; spectrometric; aeroradiometric; alteration zones

1. Introduction

The investigated area occurs in the central part of the Eastern Desert of Egypt between Latitudes 26º 18' to 26º 37' N, and Longitudes 33º 16' and 33º 51' E (Fig. 1). It is covered by a complex of Pan-African igneous and metamorphic rocks of late Proterozoic age as well as Phanerozoic sediments.

Among the rocks hosting uranium and thorium mineralizations, the late-tectonic younger pink granites show higher potentiality for carrying radioactive minerals (El Shazly et al. 1968). The radiometry exploration, which carried out by the Egyptian Nuclear Materials Authority, led to discovery of some important occurrences of radioactive mineralizations in the Eastern Desert. Many pronounced radioactive anomalies have been recorded in the study area especially in the younger granitic plutons, for example, Gabal El Erediya (El Kassas 1974), Gabal El Missikat (Bakhit 1978, Bakhit and El kassas 1989), Gabal Kifri (El Tahir 1978), Gabal Kab Amiri, Gabal Abu Aqarib and Gabal El Himeiyir (Ammar 1993).

The investigated area has been surveyed by Aero Service (1984) using high sensitivity airborne gamma-ray spectrometric and magnetic methods. This study aimed to apply different image processing techniques of Landsat ETM+ and aeroradiometric survey data for radiometric explorations of the investigated area.

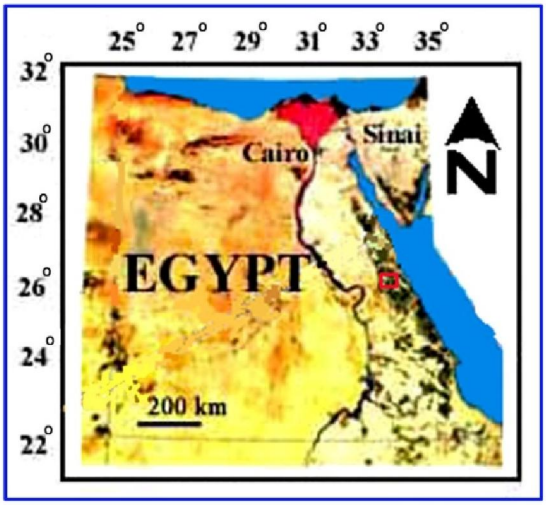

Figure 1. Location map of the study area, Central Eastern Desert, Egypt.

The geological map of the investigated area is interpreted in this work from the Landsat ETM+ image, as well as from the previous published geological maps and field investigations. The structural mapping carried out using the new established method of the automatic lineaments extraction from the digital satellite imageries. The automatic lineaments extraction is a new approach in PCI package which used recently by some authors (Leech et al. 2003, Mostafa and Bishta 2004, Bishta 2004, 2008 & 2010, Bishta et al. 2010).

2. Methodology

The following data of the investigated area are used in this work:

- Previous geological maps (scale 1: 250,000 & 1: 500,000).
- Previous topographic contour map (scale 1: 50,000).
- Landsat-7 multispectral and panchromatic ETM+ data.
- Aeroradiometric survey data.

The study area is covered by Landsat-7 Enhanced Thematic Mapper (ETM+) data. This sensor has eight broad spectral bands, six of them were detected as visible bands (1, 2 & 3), near infrared "NIR"

band (4) and short wave infrared "SWIR" bands (5 & 7). These bands have a spatial resolution of 30 x 30 meters. Band–6, which detects thermal radiation, has a spatial resolution of 60 x 60 meters. The panchromatic band-8 has a higher spatial resolution1 of 5x15 m. The used digital ETM+ raw-data was processed using special commercial software packages of remote sensing and Geographic Information System GIS, such as PCI-Geomatica-9, and Erdas Imagin-9.1. These processes are carried out for constructing lithologic and structural maps of scale 1: 100,000 of the investigated area.

Raw digital satellite data usually includes geometric distortions due to sensor geometry, scanner, platform instabilities, earth rotation, earth curvature, etc. and it is necessary to correct and adapt them (Mather, 1987, Sabins, 1997, Lillesand et al., 2004, Richards, 1995).

Geometric correction is carried out for the digital data of ETM+ bands of the investigated area through two main steps. The first step includes rectification of a panchromatic ETM+ band-8. While the second step includes rectification of multispectral, ETM+ bands (1 to 7). The correction processing in the first step carried out by collecting well distributed 75 ground control points selected from the topographic sheets (scale 1:50,000) for the investigated area using image to map method. The overall accuracy of the transformation is indicated by the average of the errors in the reference points, root mean square error (RMS = 0.63, Bernstein 1978). The cubic interpolation method is used in the resampling processing. The rectified panchromatic ETM+ band is then used as a georeferenced base for the correction of the 6-multispectral ETM+ bands (1 to 7) in the second step using image-to-image method. The following parameters are used in the registration procedures: UTM Projection, Zone 37N, and Row 42.

3. Image Processing of Landsat-7 ETM+ Data

The image enhancement is the procedures of making a raw image to be more interpretable for a particular application (PCI, 2003). The histogram equalization enhancement technique is applied to the ETM+ data of the study area to increase the contrast in the images (Schowengerdt 1983, Curran 1985, Mather 1987, Lechi 1988).

The optimum spectral band combination is determined by terrain, climate and the nature of the interpretation (Sabins 1997). The optimum False Color Composite (FCC) Landsat image of the investigated area of scale 1: 100,000 is constructed from bands 7, 4 and 2 displayed in red green and blue respectively (Fig. 2). This FCC image is used as a base image for the purposes of helping in lithologic discrimination and structural mapping of the study area. The spectral capabilities of the ETM+ bands are used to determine the best discrimination of the lithologic units and structural interpretation.

The geological map of the investigated area (Fig. 3) is interpreted from the FCC Landsat ETM+ image and field investigations. The late-tectonic younger granites, the syntectonic older granites (diorites and granodiorites) and acidic Dokhan volcanics, as well as the Phanerozoic sediments are delineated and identified by their lighter brown color. The dark colored tones distinguish the metavolcanics, metasediments and the mafic-ultramafic rocks. The Landsat ETM+ data is not much powerful in identifying and separating most the studied rock units due to its low spatial and spectral resolutions. This limitation is overcome by integrating the airborne gamma-ray spectrometric survey data technique.

4. Geologic Setting

The geological base map (Fig. 3) is prepared by interpreting the FCC Landsat image of scale 1: 100,000, with the help of field check and the previously prepared geological maps of Bakhit 1978, Bakhit and El Kassas 1989, El Ramly 1972 and Habib 1982 & 1987. These maps have been digitized and constructed using Geomatica PCI software package.

The different rock units shown on the geological map (Fig. 3) are described as follow: the metasediments and the metavolcanics, which

represent the island-arc assemblage; the serpentinites, the metagabbro, the metadiabase, the metabasalts and the amphibolites represent the ophiolitic assemblages. Those assemblages were later on intruded by the calc-alkaline older syntectonic granitoids (ranging in composition from diorite to granodiorite and granites). The Dokhan volcanics represent younger volcanicity extruded these granitoid rocks and formed mainly of dacite to rhyolitic composition with their pyroclastics with subordinate basic composition. The Hammamat sediments deposited after the Dokhan volcanics. The younger late-tectonic granites were the last igneous activity present in the study area. Several rock varieties of these younger granites are present and intruded the mapped Pan-African rock units. The Phanerozoic sediments were deposited unconformable over the above mentioned Pan-African rock units.

It is easy to distinguish on the constructed FCC Landsat ETM+ image between the late Proterozoic granitic rocks, volcanic and sedimentary rocks, as well as the undifferentiated Phanerozoic sediments. It is worthy to mention that most of the detected radioactive anomalies are restricted to the rock varieties of the younger granites. Few of the radioactive occurrences were affiliated to exposure of the upper Cretaceous phosphate beds. So, detailed spectrometric studies have been emphasized on the younger granitic rocks.

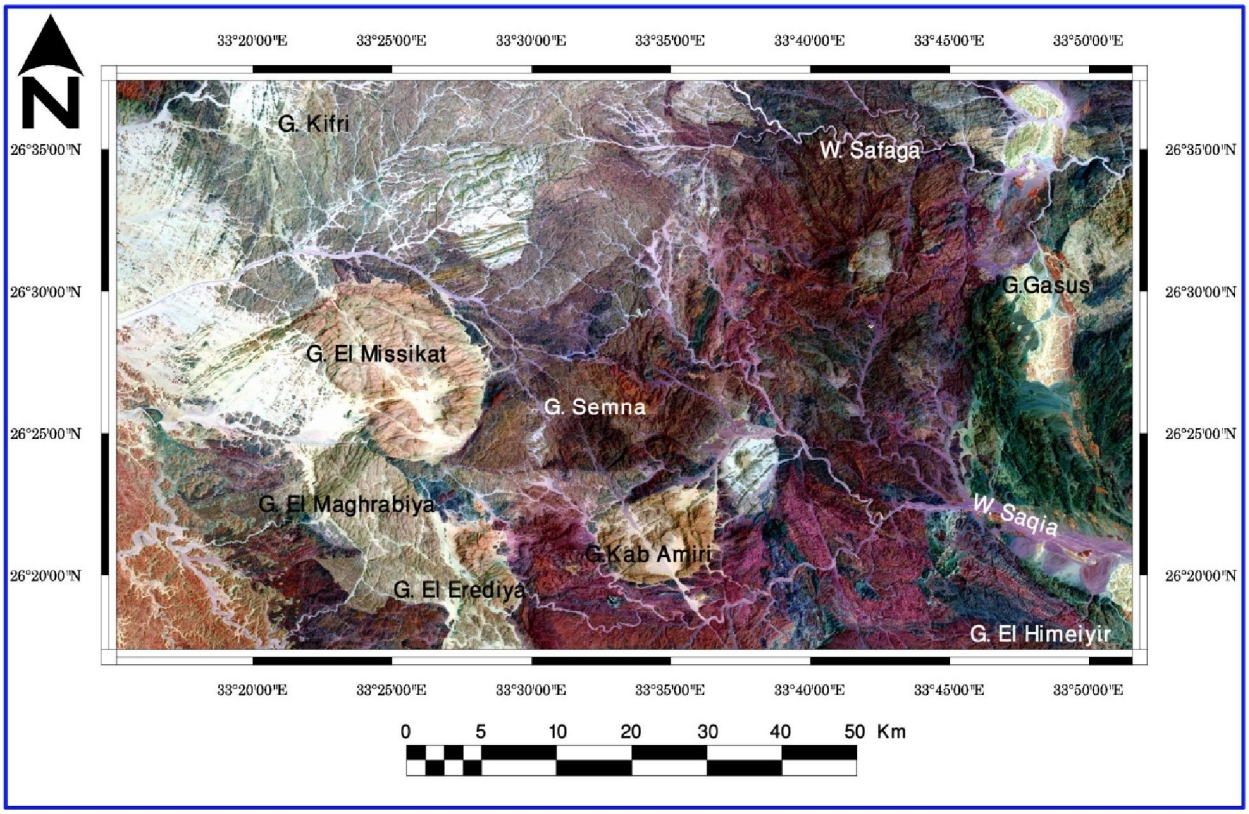

Figure 2. False color composite Landsat image, ETM+ bands 7, 4, 2 in RGB, Central Eastern Desert, Egypt. (Original scale 1:100,000)

5. Structural Lineaments Extraction

Automatic lineaments extraction from the digital remotely sensed data of Landsat 7 ETM+ is carried out using Geomatica PCI package. The different ETM+ multispectral bands (visible, NIR and SWIR bands) are tested in the automatic extraction of lineaments (Table 1), to select the optimum band for the lineaments extraction. Landsat ETM+ band 7 scored the highest number of extracted lineaments (2145). So, the automatically extracted lineaments in this work are carried out using ETM+ band 7. The automatically lineaments extraction algorithm of Geomatica PCI software consists of edge detection thresholding and linear extraction steps. The steps of lineaments extraction are carried under the defined user parameters. Table 2 shows the difference between these parameters and the default parameters of the "Geomatica PCI" package.

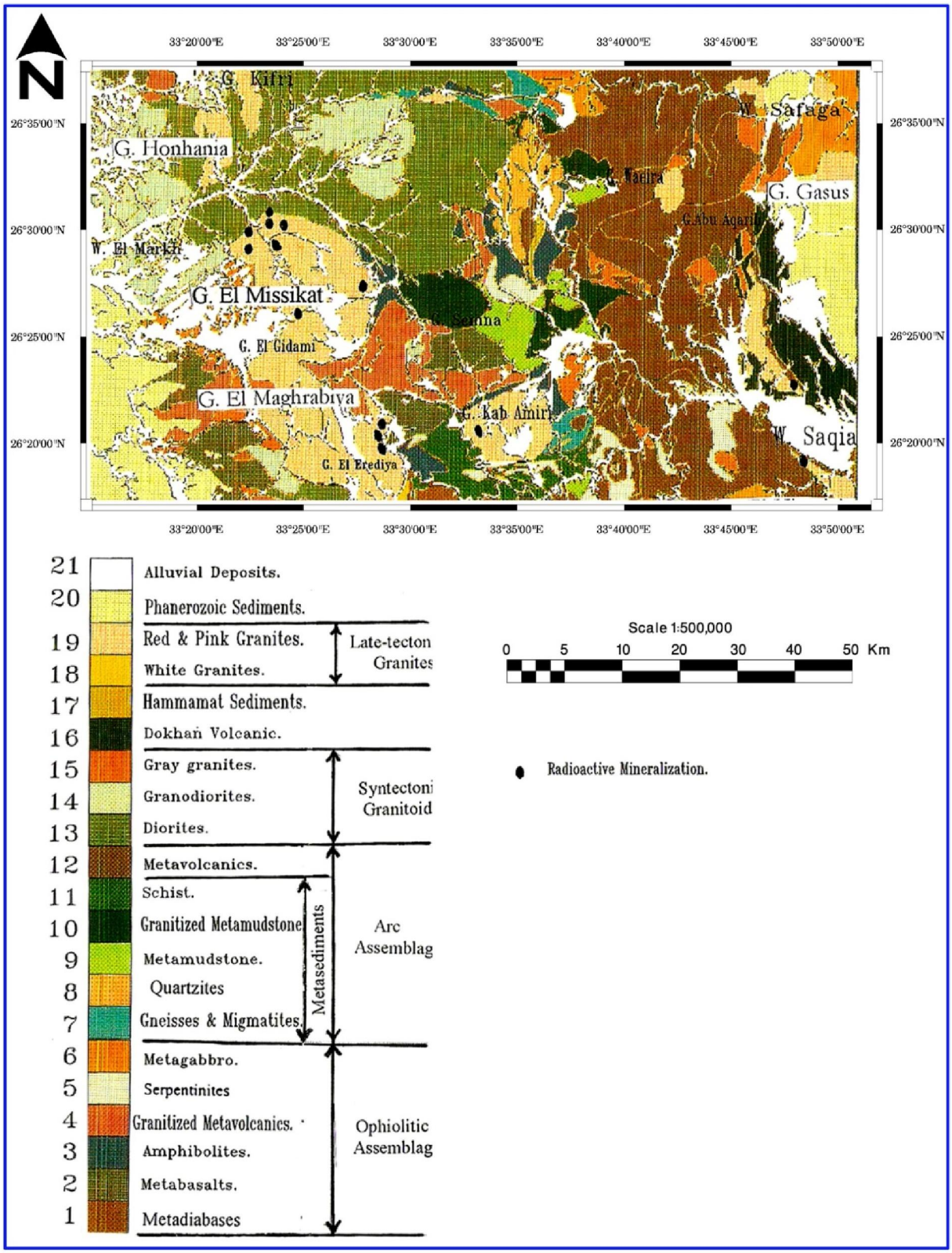

Figure 3. Geological map interpreted from Landsat ETM+ image and field investigations, Central Eastern Desert, Egypt. (Original scale 1:100,000)

Table 1. Landsat ETM+ multispectral bands versus the automatic extracted lineaments frequency, central Eastern Desert, Egypt.

ETM+ Bands	Spectral Range	Extracted lineaments (Frequency)
Band-1	Visible Blue	1352
Band-2	Visible Green	1743
Band-3	Visible Red	1552
Band-4	NIR	1633
Band-5	SWIR	1895
Band-7	SWIR	2145

Table 2. Default and user parameters used for automatic extraction of lineaments in PCI Package.

PCI Parameters	Default Values	User Values
Edge filter radius	3 (Pixels)	2 (Pixels)
Minimum edge gradieny	15 (Pixels)	10 (Pixels)
Minimum line length	15 (Pixels)	10 (Pixels)
Line fitting tolerance	2 (Pixels)	4 (Pixels)
Maximum angular difference	10 (Degree)	10 (Degree)
Maximum linking difference	30 (Pixels)	25 (Pixels)

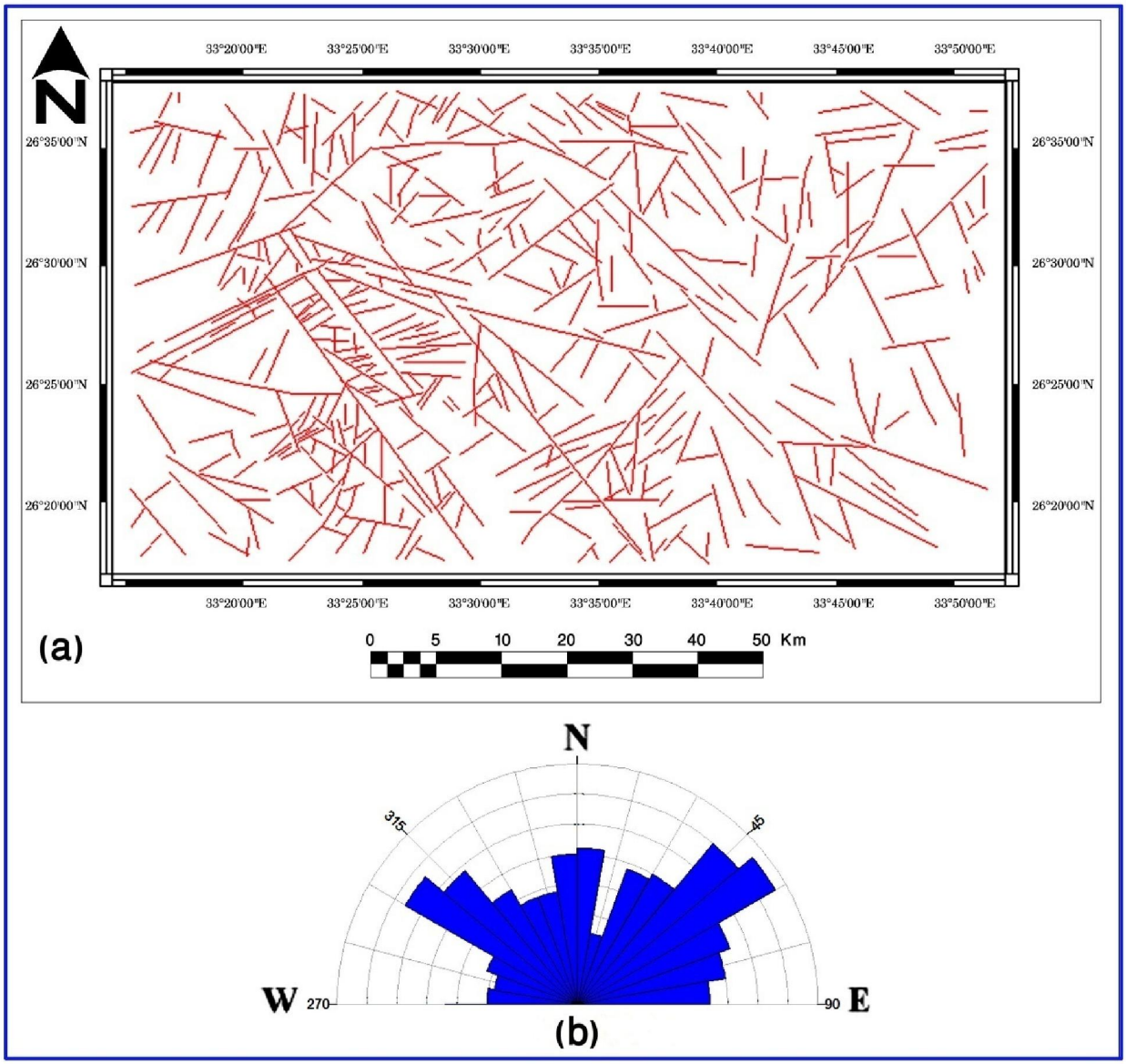

Figure 4. (a) Structural lineaments map extracted from landsat ETM+ image, and (b) Rose diagram showing the frequency lineaments trend.

The obtained automatically extracted lineaments patterns over ETM+ band-7 are visually edited on screen to delete all the false traced lineaments and check all the true structural lineaments. The final automatically structural lineaments map of the study area after editing is shown in Figure (4a). The statistical analyses of these significant structural lineaments of the investigated area have three main predominant trends in the NE-SW, NW-SE and N-S directions (as shown in the rose diagram (Fig. 4 b).

It is found that these extracted structural trends of the study area, as interpreted from the digital Landsat ETM+ data during this research, are largely coincides with the main trends defined in the geological mapping of previous literatures.

The interpretation of extracted structural lineaments (Fig. 4) and field verifications revealed that, most of the radioactive anomalies in the younger granitoids are located along the intersections of the NE with NW and N-S lineament trends. As the frequency and the intensity of these lineaments increase, the radioactive anomalies spread over larger areas as in the case of the southern part of Gabal Kab Amiri, Gabal El Missikat and Gabal El Erediya.

6. Image Processing of Airborne Gamma-Ray Spectrometry Survey Data

The image processing technique is used in constructing gamma-ray spectrometry color raster maps of K, eU, eTh and Total Count (TC). It is also used in constructing a radiometric ternary maps of K, eU and eTh (linear stretched and histogram equalized).

6.1. Color Raster Maps

The raw data of the airborne spectrometric contour maps of Aero Service (1984) are digitized at 500 m cell size and processed to construct gamma-ray spectrometric color raster maps of K, eU, eTh and TC (Figs. 5, 6, 7 & 8 respectively), using the software packages of Ilwis and Geosoft.

The color raster potassium map (Fig. 5) is distinguished to some extent between the different mapped rock units according to their K-content. This map is more helpful in differentiating and mapping the different units of granitic rocks while, it failed in differentiation between the other rock units. The color raster maps of eU, eTh and TC (Figs. 6 to 8) are helpful in determining the zones of high radioactivities, which are confined to the different rock varieties of the late-tectonic younger granitic intrusions and the phosphatic Phanerozoic sediments. On these maps, the biotite monzogranites of Gabal Kab Amiri, the biotite and leucocratic granites of Gabal El Missikat and Gabal El Erediya; the less evolved granodiorite and monzogranites of wadi El Markh; and the alkali feldspar granites of Gabal Abu Aqarib and Gabal El Himeiyir are distinguished by either enrichment in U and / or Th (Figs. 3, 6, 7 & 8).

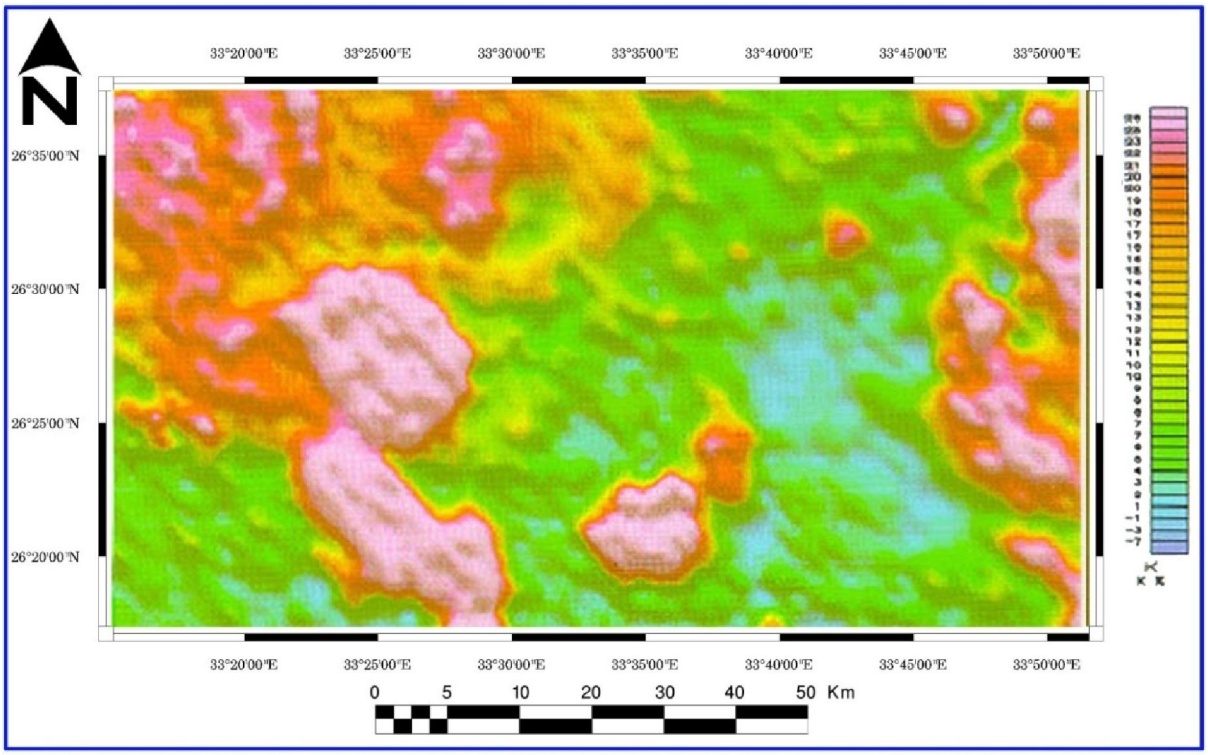

Figure 5. Color raster map of aeroradiometric potassium percents (K%), Central Eastern Desert, Egypt.

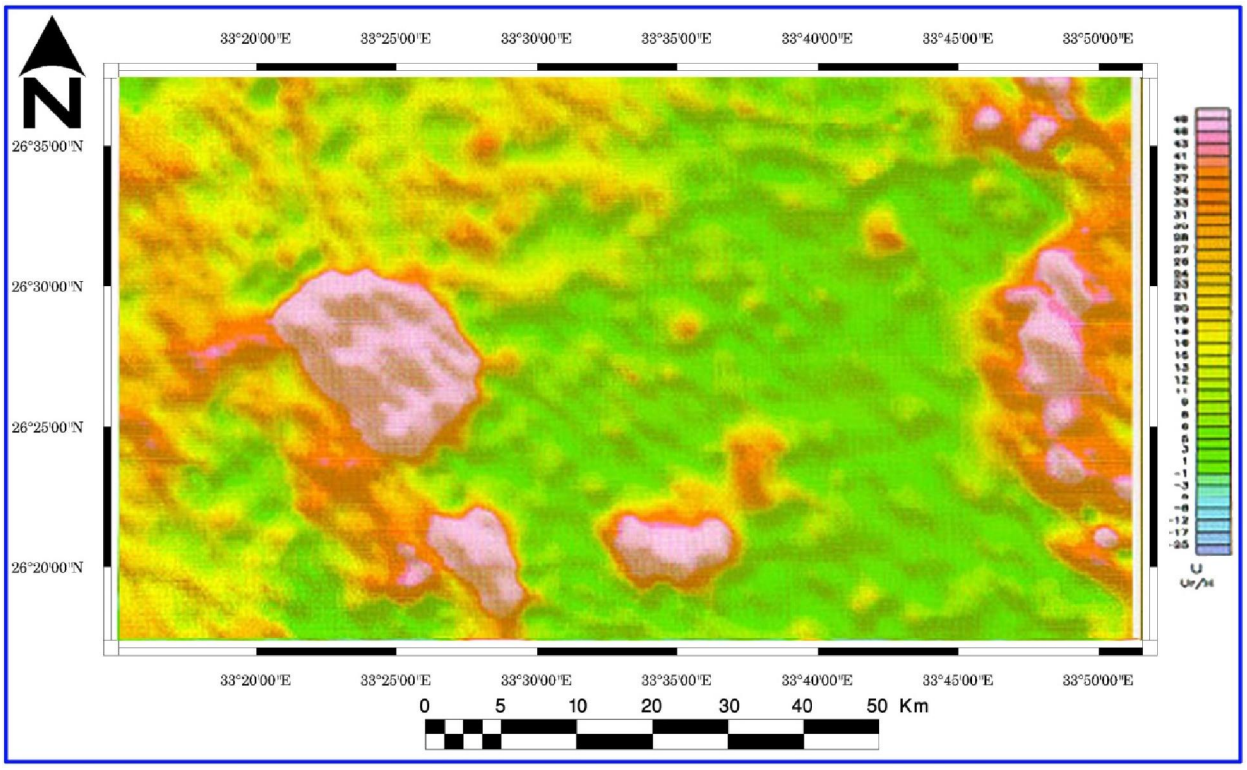

Figure 6. Color raster map of aeroradiometric equvalent uranium (eU), Central Eastern Desert, Egypt.

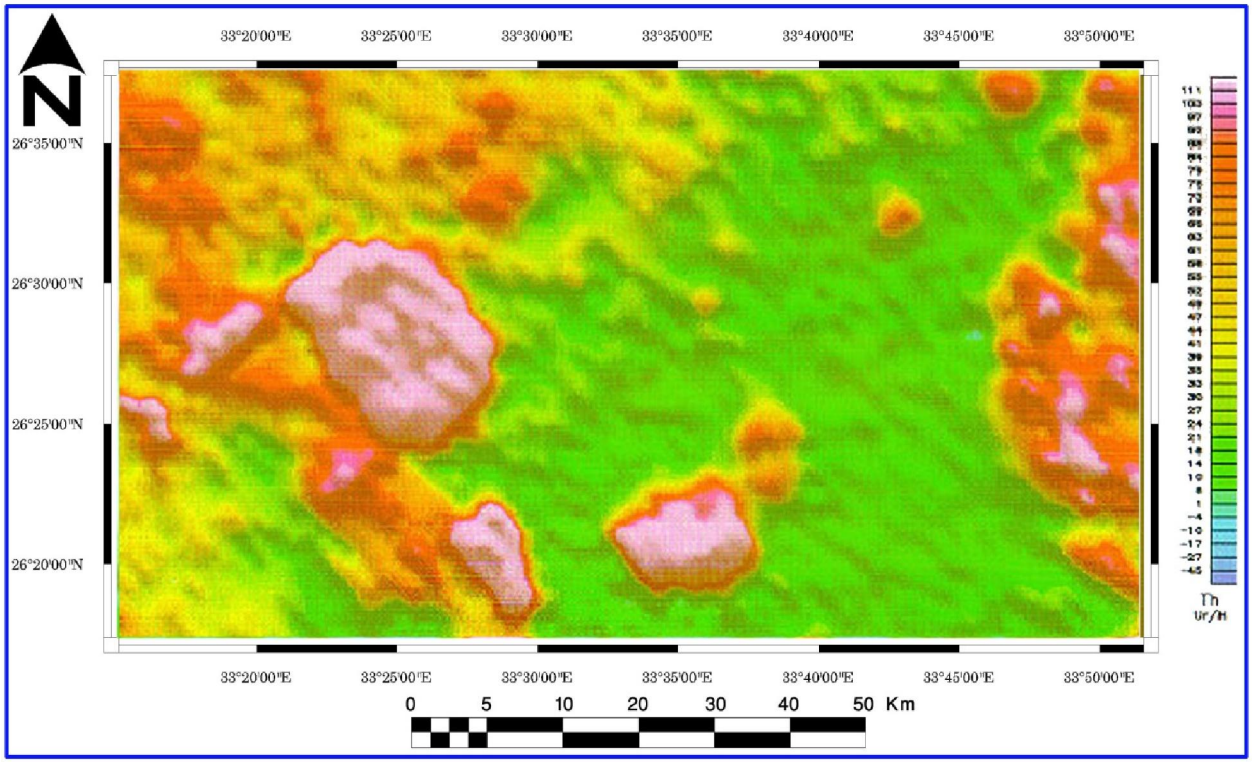

Figure 7. Color raster map of aeroradiometric equvalent thorium (eTh), Central Eastern Desert, Egypt.

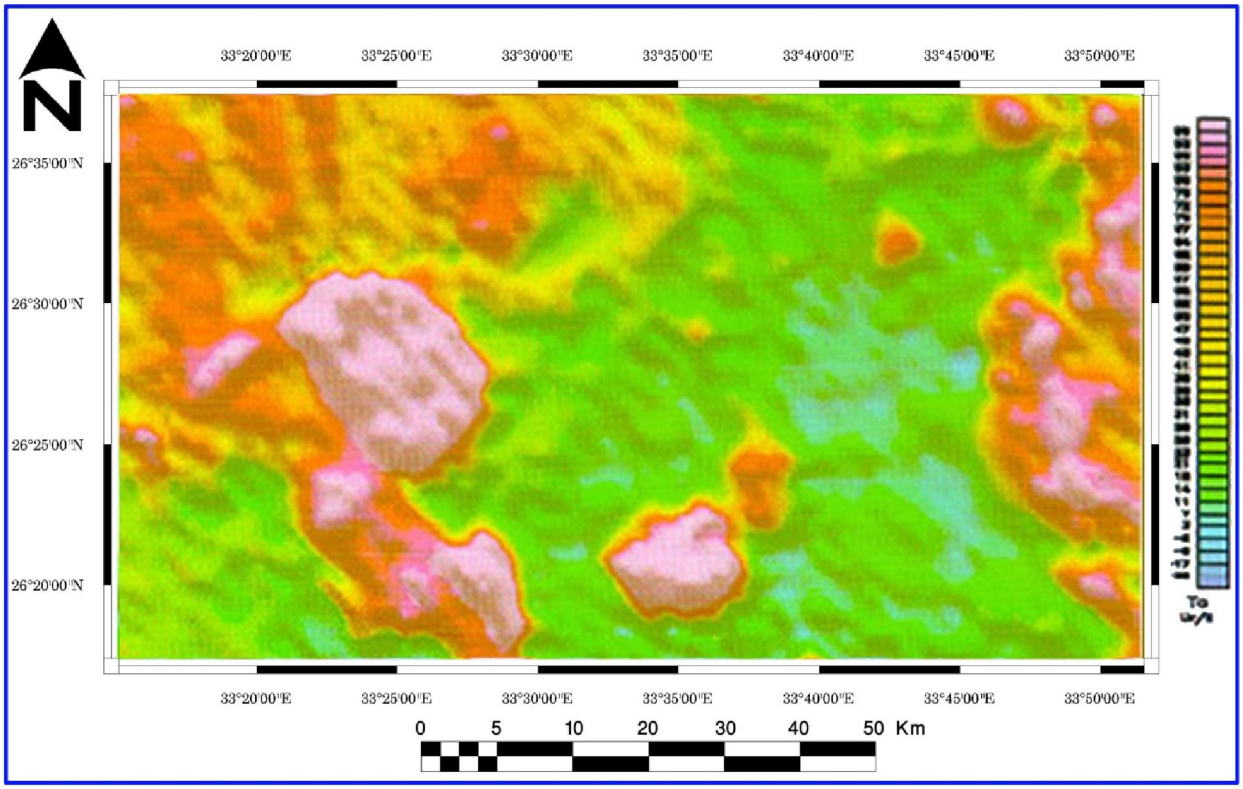

Figure 8. Color raster map of aeroradiometric total count (TC), Central Eastern Desert, Egypt

6.2. Ternary Maps

Recently, one of the most common practices in presenting gamma-ray spectrometric data is to produce a color ternary map, i.e., a color composite in image processing terminology. This is carried by assigning each of the three radioelements K, eTh and eU to one of the primary colors. On a computer screen, the convention is to describe potassium (K) to red, equivalent thorium (eTh) to green and equivalent uranium (eU) to blue. After individually de-stripping each raster to remove as much flight-line-related "noise" as possible without reducing the "signal", each channel is histogram-equalized and the three radioelements are presented together as a color image. Here, it is seen that such processing gives pictures principally of surface lithology and secondarily of surface structures, both in characteristic colors and of outstanding clarity.

The constructed colored enhanced linear stretched ternary map (Fig. 9) using the image processing technique shows five different radioactive units (five-color groups). These color groups are reflecting the concentration of the three radioelements (K, eU and eTh) in the mapped area, as shown in Table 3. These five radioactive units are the R1 (cyan = eU + eTh), R2 (green = eTh), R3 (yellow = K + eTh), R4 (red = K) and R5 (magenta = K + eU). The ternary map (Fig. 9) shows that these different color groups pigmented areas covered by granitic rocks (older and younger), acidic Dokhan volcanics and some parts of Phanerozoic sediments. The study showed that this map is very helpful in distinguishing the potassium-enriched rocks and those having different concentrations of the radioactive elements (eU and / or eTh), as well as the anomalous U-concentrations in the area.

Table 3. Radiometric units interpreted from the linear stretched aeroradiometric ternary map, central Eastern Desert, Egypt.

Radiometric Unit	Color on ternary map	Indicated Radioelement	Occurrence
R1	Cyan	eU & eTh	Northern part of G. El Missikat
R2	Green	eTh	South Kab Amiri, G. El Missikat, West G. El Missikat (W. El Markh), G. El Erediya (Northern part), G. Kifri (Northern part), G. Abu Agarib
R3	Yellow	K & eTh	G. Kab Amiri and G. El Missikat
R4	Red	K	G. El Maghrabiya, G. El Gidami, North G. Kab Amiri and G. Kifri
R5	Magenta	K & eU	G. El Erediya, G. El Missikat and upper cretaceous phosphatic beds of W. Safaga and G. Gasus.

The younger granites on the linear stretched ternary map are all pigmented by the red color R4-type (K-enriched). They differ in composition

according to the variation of the modal percentage of K-feldspar to plagioclase feldspar.

Though some plutons in the study area show anomalous varieties in the radioelements with the pluton itself. An example is Gabal El Missikat (Figs. 3, 9 & 10) which comprise more than varieties from R3 (enriched K and Th) to R1 (enriched in U and Th). This is in agreement with the recently discovered uranium occurrence in the northern part of the pluton. Another example is Gabal Kab Amiri, which varies from the R4 (K-enriched) in the north to R2 (Th-enriched) in the southern part.

Generally, the ternary map (Fig. 9) pointed out to some important uranium anomalous zones such as those at Gabal Kifri, Wadi El Markh, Gabal El Missikat, Gabal El Gidami, Gabal El Maghrabiya, Gabal Kab Amiri, and Gabal Abu Aqarib. Moreover, the linear stretched ternary map (Fig. 9) shows a uranium anomaly on the eastern part of the study area (R5-type). This zone was found to be related to the phosphatic beds in the Phanerozoic sedimentary cover.

The main features of the anomalous zones in the present study area are summarized and presented in Table 4. This Table shows that, 10 radioactive anomalous zones are characterized in this work.

The first two zones are encountered in the YG1 granitic type of Gabal Kifri and Wadi El Markh (zones No. 1 & 2). The host rock types are tonalite granodiorite monzogranite. The anomalous zones of this type (YG1) show mean values of K 2.15-2.45%, eU 3.06-3.59 ppm and eTh 8.11- 8.46 ppm (R4-type). The mineralized zones, caused by aplitic, felsitic and pegmatite intrusive exhibit mean values reaching up to eU 4.79 ppm and eTh 10.87 (zone No. 1, R2-type, at wadi El Markh) and eU 4.26 ppm and eTh 9.41 (Zone No. 2, R2-type, at Gabal Kifri). Zones No. 3 and 4 of Gabal Abu Aqarib and Gabal El Himeiyir are encountered in YGII type. The host rock types are alkali feldspar granites. The anomalous zones of this type show mean values of K 2.54-2.68%, eU 4.81-5.1 ppm and eTh 10.9- 11.58 (R4-type). The mineralized zones (R2-type), caused by silica (quartz) veins, reach up to eU 5.17 ppm and eTh 11.71ppm (as in Gabal Abu Aqarib, zone No. 3) and up to eU 5.05 ppm and eTh 11.47 ppm (as in Gabal El Himeiyir, Zone No. 4).

The anomalous zones No. 5, 6, 7, 8, and 9 are encountered in the YGIII type. The host rock types are monzogranites – biotite and leucocratic granites and microgranites. These zones show mean values of K% 2.77, eU 5.58 ppm and eTh 12.42 ppm (R4-type). The mineralized zones, invaded by biotite, leucocratic and microgranite dykes, exhibit mean values reaching up to eU 5.6 ppm and eTh 12.54 (as in southern part of Gabal Kab Amiri, R2- & R3-types, zone No. 5), eU 6.27 ppm and eTh 14.16 ppm (Gabal El Maghrabiya, R2-type, Zone No. 6); and eU 6.4 ppm and eTh 14.3 ppm (Gabal El Gidami, R2- & R5-types, zone No. 7). The mineralized zone which is characterized by the invasion of siliceous and jasperoid veins exhibit mean values of eU 6.21 ppm and eTh 13.7 ppm (Gabal El Missikat, R1-, R2- & R5-types, zone No. 8); and eU 6.01 and eTh 13.5 ppm (Gabal El Erediya, R5- & R2-types, zone No. 9).

The high radioactive upper Cretaceous phosphatic beds of Duwi formation (R5-type, zone No. 10) exhibits mean values of K 0.96%, eU 2.77 ppm and eTh 5.34 ppm and located at Wadi Safaga and Gabal Gasus (Figs. 3 & 9).

The different applied techniques during this study indicate that most of the radioactive anomalies are confined to the intrusion of the late tectonic younger granites. The later introduced uranium bearing solutions are structurally controlled by the fracture systems cutting across the granites. The granitic rocks enclosing the radioactive mineralization are partially altered through sericitization, kaolinization, hematitization and silicification. These altered granitic rocks carry fluorite and sometimes garnet. Other anomalies are associated in the sedimentary cover Cretaceous phosphatic beds.

7. Discussion

The high radioactive anomalies are mostly restricted to the late-tectonic younger granitic rocks of the study area. The ternary map (Fig. 9), differentiates the younger granitic rocks into five colors pointing to five radioactive rock units- R1, R2, R3, R4 & R5 (Fig. 10). The field investigation distinguished the late-tectonic younger granites of the study area to coarse-grained rosy biotite monzogranites; more evolved pink to red colored biotite and leucocratic granites; and alkali feldspar granites. Does the five radioactive rock varieties that shown on the ternary map (Fig. 9) mean five different petrological and mineralogical rock varieties? At least this difference indicates relative enrichment in the radioelements (K, U and Th). However, all the late-tectonic younger granitic rocks on the color raster potassium map (Fig. 5) give pink color, which reflects their characteristic high percentage of K relative to the other studied rocks. The color raster potassium map is not able to distinguish between the five different rock varieties of the younger granites shown on the ternary map. The petrographic investigation will be discussed to distinguish the mineralogical difference (if present) within the late-tectonic younger granite rock units, and to understand the meaning of the existence of the proposed five radioactive rock varieties that shown on the ternary map (Fig. 9).

The analyzed samples from Gabal Abu Aqarib and Gabal El Himeiyir fall in the alkali feldspar field,

while samples from Kab Amiri, El Maghrabiya and El Gidami fall in the monzogranite field. The samples from the Gabal El Missikat and Gabal El Erediya fall also in the monzogranite field but are characterized from those of Kab Amiri by more leucocratic and finer in grain size, so they distinguished in this work by naming biotite granite and leucocratic granite.

The petrographic investigation can differentiate the late-tectonic younger granitic rocks of the study area into four main types. The modal analyses of these rocks show that they are ranging in composition from granodiorite (with tonalite and monzogranite) type (Gabal Kifri, Gabal Honhania and wadi El Markh) to monzogranite type (Gabal Kab Amiri, Gabal El Maghrabiya and Gabal El Gidami) to the more-evolved granitic type (Gabal El Missikat and Gabal El Erediya) and finally the alkali feldspar granite type of Gabal Abu Aqarib and Gabal El Himeiyir.

8. Conclusion

In conclusion, the results of the present study point out to several important potential areas for radioactive mineralization and to some important zones in the previously known U-mineralized localities. These parts are summarized in the following recommendations.

1 - The application of the aeroradiometric maps has limited uses in mapping the different rock units, but it is very important in defining anomalous zone and potassic rocks such as granites.

2 - The color enhanced ternary maps of airborne gamma ray spectrometric data is constructed for the investigated area. The image processing technique of the ternary map is a good tool to recognize and differentiate K-, U- and Th- bearing rocks and to locate U-anomalies.

3 - It is needed to reevaluate the exploration program of Gabal El Missikat and Gabal Kab Amiri according to the radioactive zonations proposed by the colored enhanced ternary map prepared during this study. It is recommended to carry out the exploration program at Gabal El Missikat and Gabal El Gidami as an anomalously high radioactive zone not as individual spots, as shown on Figures (9 & 10). Also the southern part of Gabal Kab Amiri can be considered as another anomalously high radioactive zone.

4- The newly reported anomalously high radioactive zones depicted by color enhanced ternary maps are checked out (e. g., the granitic rocks of Wadi El Markh, the granitic rocks in the southern part of Gabal Kab Amiri and the phosphatic beds of wadi Safaga and Gabal Gasus). Detailed investigations of these zones must be Worthwhile in future exploration in the central Eastern Desert of Egypt.

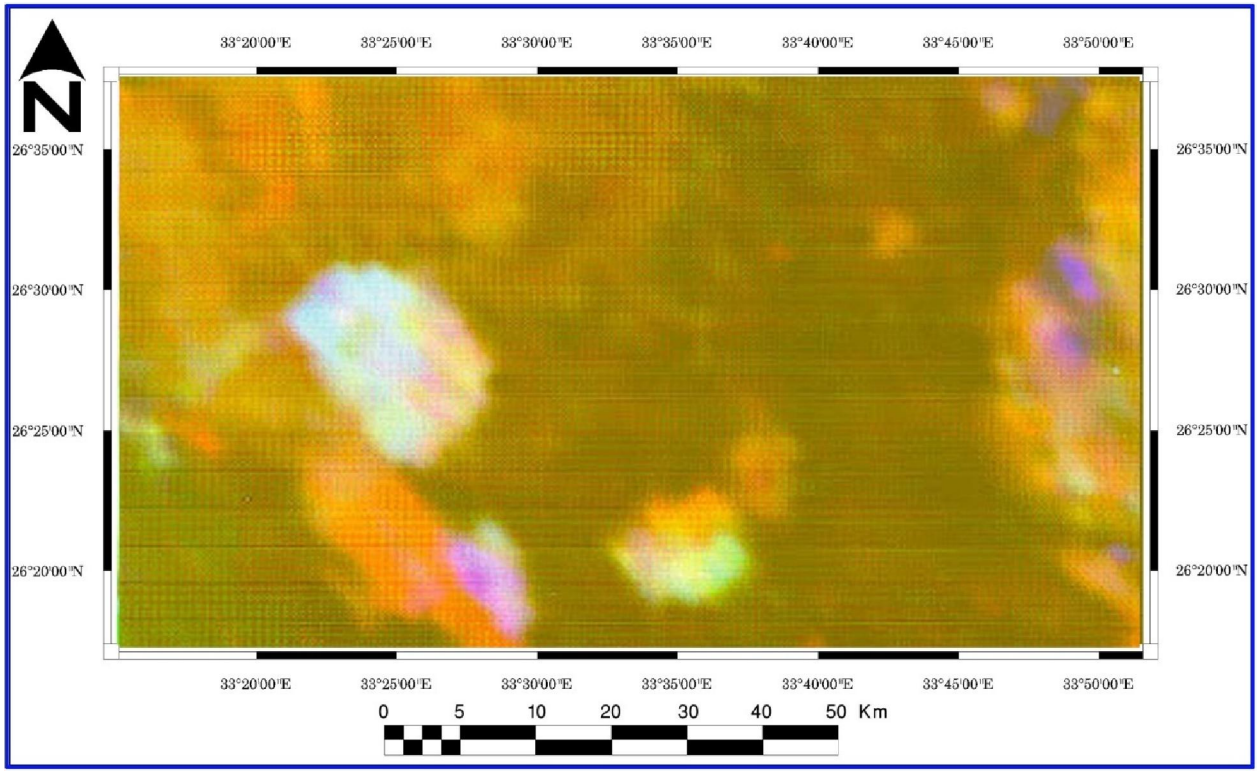

Figure 9. Color enhanced linear stretched aeroradiometric ternary map, Central Eastern Desert, Egypt

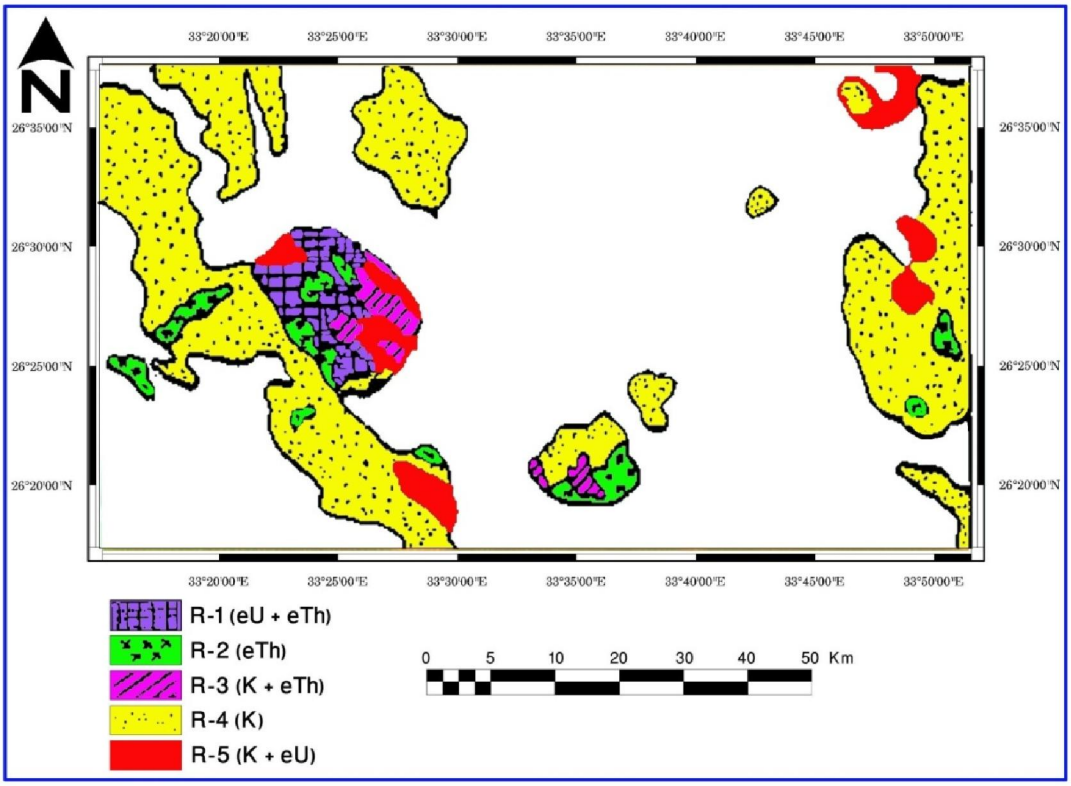

Figure 10. Radioactive rock units as interpreted from linear stretched aeroradiometric ternary map, Central Eastern Desert, Egypt

Table 4. Summary of the main features of the radioactive anomalous zones in the study area.

Anomalous Zone				Radioactivity			
Zone No.	Host rock types	Locality	Mode of occurrence	Radioactive type on ternary map	K %	eU ppm	eTh ppm
10	Upper Cretaceous Duwi formation	* Wadi Safaga & * G. Gasus	Phosphatic Beds	R5	0.96	2.77	5.34
9	Biotite and Leucocratic Granites and Microgranites (YGIII)	G. El Erediya	Jasperoid veins	R5 & R2	2.77	6.01	13.5
8		G. El Missikat	Siliceous veins	R1, R2 & R5	2.71	6.21	13.7
7	Morzogranites (YGIII)	G. El Gidami	Leucocratic granitic and Microgranitic dykes	R2 & R5	2.77	6.4	14.3
6		* G. El Maghrabiya	Leucocratic granitic and Microgranitic dykes	R2	2.76	6.27	14.16
				R4	2.78	5.79	12.89
5		* G. Kab Amiri (southern part)	Pegmatite	R2 & R3	2.77	5.6	12.54
				R4	2.77	5.58	12.42
4	Alkali Feldspar Granites (YGII)	G. El Himeiyir	Quartz Veins	R2	2.60	5.05	10.9
				R4	2.54	4.81	11.71
3		G. Abu Agarib	Quartz Veins	R2	2.68	5.17	11.58
				R4	2.68	5.1	13.5
2	Tonalite-Granodiorite Morzogranite (YGI)	G. Kifri	Pegmatite and felsitic dykes	R2	2.54	4.26	9.41
				R4	2.45	3.59	8.11
1		* Wadi El Markh	Aplitic Dykes	R2	2.53	4.79	10.87
				R4	2.15	3.06	8.46

R1 = enrichment of eU and eTh
R2 = enrichment of eTh
R3 = enrichment of K and eTh
R4 = enrichment of K
R5 = enrichment of K and eU

* New zones of radioactive anomalies

Correspondence to:
Prof. Adel Zein Bishta
Faculty of Earth Sciences, King Abdulaziz University.
Jeddah, P.O. Box: 80206 Jeddah: 21589, Saudi Arabia
Telephone: +966530911301
Emails: abishta@kau.edu.sa or adel_zein2@yahoo.com

References

1. Aero Service. Final operational report of airborne magnetic radiation survey in the Eastern Desert, Egypt. Conducted for the Egyptian General Petroleum Corporation. Aero Service, Houston, Texas, April 1984, six volumes.
2. Ammar SE. Geological, structural and geochemical investigations of Kab Amiri-Wadi El Saqqia area and its radioactive occurrences, Central Eastern desert, Egypt. Ph. D. Thesis, Cairo Univ., Egypt, 1993, 285.
3. Bakhit FS. Geology and radioactivity mineralization of G. El Missikat area, Eastern Desert, Egypt. Ph. D. Thesis, Ein Shams Univ., Egypt, 1978, 289.
4. Bakhit FS and El Kassas IA. Distribution and orientation of radioactive veins in the El Erediya-El Missikat area, Central Eastern Desert, Egypt. Int. Jour. Remote Sensing, 1989, 10: 565-581.
5. Bernstein, R. Digital image processing for remote sensing, Wiley, New Yourk, 1978.
6. Bishta A. Z Lithologic discrimination of Gabal Qattar-Um Disi environs, north Eastern Desert of Egypt using thematic mapper data of Landsat-7. The third International Symposium on Geophysics, Tanta University, Tanta, Egypt, 2004, 541-557.
7. Bishta AZ Lithologic discrimination using selective image processing techniques of Landsat-7 data, Um Bogma environs, Westcentral Sinai, Egypt, JKAU: Earth Sci, 2008, 21: 193-213 (2009 A.D. /1430 A.H.).
8. Bishta AZ. Assessing utilization of multi-resolution Satellite imageries in geological mapping, a case study of Jabal Bani Malik area, eastern Jeddah city, Kingdom of Saudi Arabia, JKAU: Earth Sci, 2010, 21: 27-52 (2010 A.D. /1431A.H.).
9. Bishta, A.Z., Mohamed A. Soliyman, Ahmed A. Madani and Mohamed A. Abu Qudaira. Utilization of lineaments extraction from satellite imageries in structural mapping and mineral exploration of central Wadi Araba, Southwest Jordan. JKAU: Earth Sci, 2010, 2: 1-27.
10. Curran, P. J. principles of Remote Sensing. Longman.New Yourk, 1985.
11. El Kassas I. A. Radioactivity and geology of Wadi Atalla area, Eastern Desert of Egypt, A.R.E Ph. D, Thesis, Ein Shams Univ., Egypt, 1974, 502.
12. El Ramly M. F. A new geological map for the basement rocks in the Eastern and southwestern Desert of Egypt, scale 1: 1000,000. Ann. Geol. Surv., Egypt, 1972, 2: 1-18.
13. El Shazly EM, Shukri NM, Fouad KA, Ammar AA and Meleik M. L. Airborne radiometry and regional geology in the Central Eastern Desert, Egypt, UAR. Int. Geol. Congr. Prague, 1968, 5: 37-48.
14. El Tahir M. A. Relation between geology and radioactivity of some basement rocks, to the north of Qena- Safaga asphaltic road, Eastern Desert, Egypt. M. Sc. Thesis, Al Azhar Univ., Egypt, 1978, 148.
15. Habib M. E. Landsat investigation of mineralized granites in the area between Gabal El Urf and El Erediya due west of Safaga, Egypt. 8th. Int. Symp. on Machin processing of remotely sensed data, LARS / Purdue Univ., West Lafayette, U.S.A., 1982, 441-446.
16. Habib M. E. Geologic and metallogenic significance of Pan-African lineaments in the Central Eastern Desert of Egypt. Arab. Gulf. Jour. Sci. Res., 1987, 5: 59-73.
17. Leech, D.P., Treloar, P.J., Lucas, N.S and Grocott, J. Landsat TM analysis of fracture patterns: A case study from the Coastal Cordillera of northern Chile. International Journal of Remote Sensing, 2003, 24: 3709-3726.
18. Lechi, G. Satellite sensors and satellite image characteristic. Rep 11th international training course on applications of remote sensing to agricultural statistics (5-20 May 1986), Remote and Montpellier FAO, Rome, 1988.
19. Lillesand TM, Kiefer RW, Chipman J. W. Remote sensing and image interpretation. 4th ed., John Wiley and Sons Inc. New York, 2004, ISBN: 0-471-25515-7: 763.
20. Mather P. M. Computer processing of remotely sensed images, an introduction. John Wiley and Sons, 1987, ISBN: 0 – 471 – 9064 –4.
21. Mostafa, M. E. and Bishta, A.Z. Significance of lineament patterns in rock unit classification and designation: a pilot study on Gharib-Dara area, northern Eastern Desert, Egypt. International Journal of Remote Sensing, 2004, 25: 1-13.
22. PCI Geomatica, Software 9.1 helps, 2003.
23. Richards J. A. Remote sensing, digital image processing, an introduction, 1995.
24. Sabins F. F. Remote sensing: principles and interpretaion. WH freeman. New York, 1997.
25. Schowengerdt, R. A. Techniques for image processing and classification in remote sensing. Academic Press, Inc., US, 1983, ISBN: 0 – 12-62890 – 8.

11/25/2017